Check for updates

Modulation anisotropy of nanomaterials toward monolithic integrated polarization-sensitive photodetectors

Yuan Pan,† Huiru Sun,† Lingxuan Ji, Xuanxuan He, Wenzhe Dong and Hongyu Chen [ID] *

By virtue of the unique ability of providing additional information beyond light intensity and spectra, polarization-sensitive photodetectors could precisely identify targets in several concealed, camouflaged, and non-cooperative backgrounds, making them highly suitable for potential applications in remote sensing, astronomical detection, medical diagnosis, *etc*. Therefore, to provide a comprehensive design guideline for a wide range of interdisciplinary researchers, this review provides a general overview of state-of-the-art linear, circular, and full-Stokes polarization-sensitive photodetectors. In particular, from the perspectives of technological progress and the development of nanoscience, the detailed discussion focuses on strategies to simplify high-performance polarization-sensitive photodetectors, reducing their size and achieving a smaller volume. In addition, to lay a solid foundation for modulating the properties of future nanostructure-based polarization-sensitive photodetectors, insights into light–matter interactions in low-symmetry materials and asymmetric structures are provided here. Meanwhile, the corresponding opportunities and challenges in this research field are identified.

Guangdong Provincial Key Laboratory of Chip and Integration Technology, School of Electronic Science and Engineering (School of Microelectronics), Faculty of Engineering, South China Normal University, Foshan 528225, P.R. China. E-mail: chenhy@m.scnu.edu.cn
† These authors contributed equally to this work.

Hongyu Chen received her Ph.D. from the Changchun Institute of Optics, Fine Mechanics and Physics, Chinese Academy of Sciences, in 2014. Afterward, she worked as a postdoctoral fellow in the Department of Materials Science, Fudan University, China. Since then, she has worked as a lecturer in the Department of Physics, Harbin Institute of Technology, China. Currently, she is an associate professor at the School of

Hongyu Chen

Electronic Science and Engineering (School of Microelectronics), South China Normal University, China. Her current research interests include the design, fabrication, and exploration of novel properties of optoelectronic devices based on semiconductor and metallic materials, with a special focus on low-dimensional photodetectors.

1. Introduction

During the past few decades, it has been witnessed that the booming photodetectors, functioning as "electronic eyes", have transformed the way we understand the world. In particular, several special-function photodetectors not only allow us to "see" previously invisible substances (such as ultraviolet or infrared radiation), but also enable us to identify targets more precisely.[1] Notably, based on the special ability to enhance the recognition of optical information dimensions from three dimensions (intensity, spectrum, and space) to seven dimensions (intensity, spectrum, space, polarization, polarization azimuth, polarization ellipticity, and rotation direction), polarization-sensitive photodetectors could further upgrade the capacity of photodetection to improve visual contrast and acuity.[2] There is no doubt about the paramount significance of polarization-sensitive imaging techniques in fields such as remote sensing, environmental monitoring, astronomy, secure communications, medical diagnostics, autonomous navigation, and human–robot collaboration.[3–7]

So far, most of the commercial polarization-sensitive photodetectors in terms of amplitude-, time-, local area-, and focal plane-resolved technological implementations have been realized using non-monolithic approaches, in which polarizers are positioned in front of photodetectors.[8] However, under the impetus of Moore's law, the feature size of highly integrated

electronic devices has shrunk toward several nanometers.[9] Therefore, to realize a highly integrated polarization-sensitive photodetection system, it is essential to scale photodetectors down to the nanoscale. Nevertheless, conventional polarizers start to malfunction due to the optical diffraction limit when their size decreases to a sub-wavelength scale.[10] Consequently, there is an urgent need to develop techniques to resolve these contradictions. Fortunately, as a new class of building blocks, several nanostructured materials with asymmetric structures exhibiting a special quantum confinement effect, surface effect, nonlinear optical effect, and dielectric confinement effect are explored for fabricating nanostructured monolithic polarization-sensitive photodetectors, which exhibit huge potential to resolve this convoluted issue.[1,6,7,11,12] For instance, the application of nonlinear optical effects not only facilitates in-depth research into the anisotropic properties of 2D materials and the generation of circularly polarized light using chiral materials but also spurs the development of full-Stokes polarization-sensitive photodetectors based on metasurfaces.[13–16] Moreover, nanoscale metallic and half-metallic materials exhibit fascinating optical properties, which can concentrate, route, and manipulate light at a sub-wavelength scale.[9] Therefore, the potential applications of anisotropic nanostructured materials for fabricating monolithic polarization-sensitive photodetectors are truly impressive.

Up to now, extensive efforts have been made to explore the anisotropic optoelectronic properties of nanostructured materials and associated polarization-sensitive photodetectors, while a review of monolithic polarization-sensitive photodetectors involving potential materials and building blocks is still lacking. Herein, this review systematically demonstrates the current literature on photodetectors ranging from linear through circular to full-Stokes polarization-sensitive devices (Fig. 1). In particular, the polarization-sensitive photodetection technology is meticulously traced from complexity to simplicity, especially in the context of miniaturization and integration. Then, the light–matter interactions in low-symmetry materials as well as the design principles of polarization-sensitive photodetectors are described before outlining the challenges and opportunities in this area.
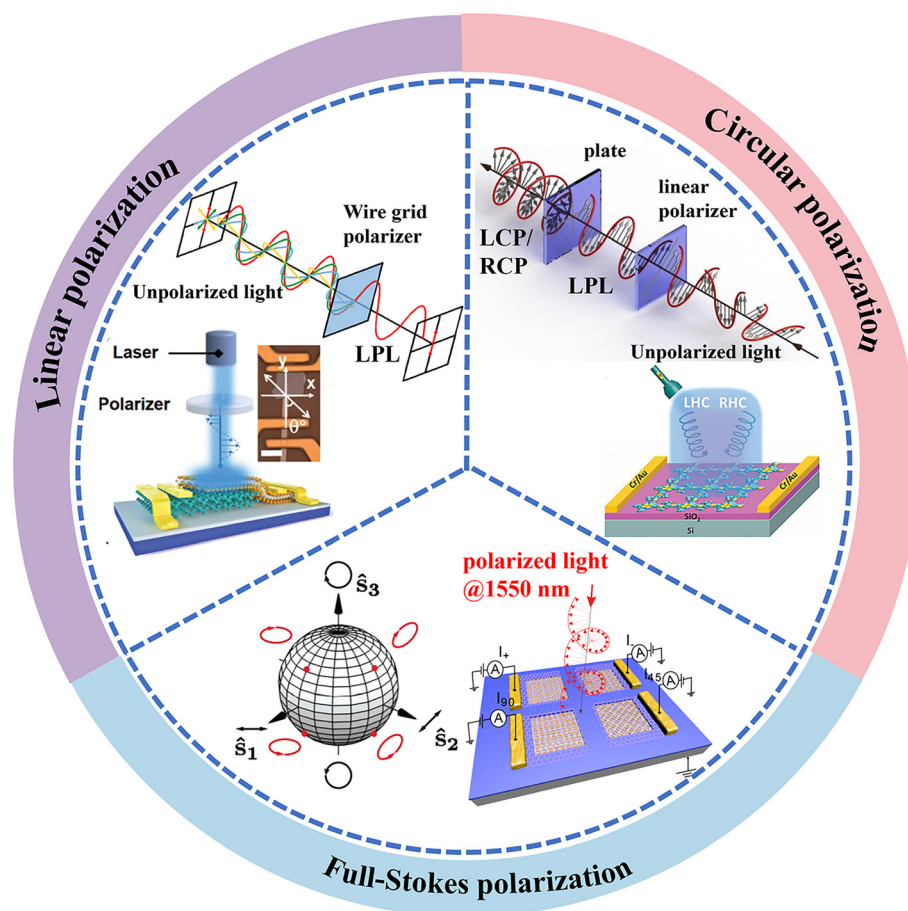

Fig. 1 The main classifications of polarization-sensitive photodetectors: linear-,[17] (copyright 2021, Royal Society of Chemistry) circular-,[18] (copyright 2023, John Wiley and Sons) and full-Stokes polarization[19,20] (copyright 2016, Optica Publishing Group and copyright 2020, American Chemical Society).

2. Polarization-sensitive photodetectors

This section deeply discusses several core research trends in the field of polarization-sensitive photodetectors, covering linear-, circular-, and full-Stokes polarization-sensitive photodetectors. The classification of these photodetectors and their typical working principles are discussed in detail. The purpose of this section is to systematically review the research progress of these polarization-sensitive photodetector technologies and emphasize their important characteristics.

2.1 Linear polarization-sensitive photodetectors

The characteristic of linearly polarized light is that its electric field vector oscillates in a plane and propagates along a straight line. The operation of linear polarization-sensitive photodetectors relies on the differences in the absorption or reflection of light with different polarization directions by materials. In addition to common photodetector parameters, the performance of linear polarization-sensitive photodetectors is particularly dependent on the polarized ratio (μ), which is the ability to respond to linearly polarized light.[6,21,22]

$$\mu = \frac{I_{max}}{I_{min}}$$

It is usually reflected in the ratio of the maximum and minimum photocurrent generated by the photodetector under differently polarized light. The higher the polarized ratio, the greater the extinction ratio of the device, and the stronger the ability to distinguish information differences.

2.1.1 Polarization-sensitive photodetectors based on micro–nano structures.
Traditional photodetectors rely on physical components, which limit their miniaturization and integration. To overcome these limitations, early on-chip integrated polarization-sensitive photodetectors incorporated specialized micro–nano structures, including plasmonic gratings and anisotropic plasmonic nanostructures, which are capable of manipulating the polarization state of light at the microscopic scale for efficient polarized photodetection. For example, an omnidirectional polarization-sensitive photodetector was proposed by Zhang et al., which is based on the design of a metamaterial absorber (MMA).[23] Metal micro–nano structures arranged periodically on the surface of the photodetector are prepared to realize the detection of linearly polarized light. Similarly, Lee et al. designed a new type of linear polarization-sensitive tunable absorber, which is composed of a dielectric–metal–dielectric multilayer structure and a plasma grating (Fig. 2a).[24] The realization of linear polarization-sensitive photodetection is based on the plasma grating structure, which can adjust the absorption rate according to the polarization state of the incident light (transverse electric mode and transverse magnetic mode). In addition, Chen et al. prepared a photodetector based on MoS$_2$, which realizes the photodetection of linearly polarized light by introducing an anisotropic plasmonic nanostructure (Fig. 2b).[25] The maximum and minimum photocurrent ratio of this structure in two perpendicular polarization directions reaches 1.45, which proves that the polarization sensitivity induced by anisotropic nanostructures provides a new method for the fabrication of polarization-sensitive photodetectors. These constructs represent innovation and progress in linear polarization-sensitive photodetectors. However, they face challenges such as the
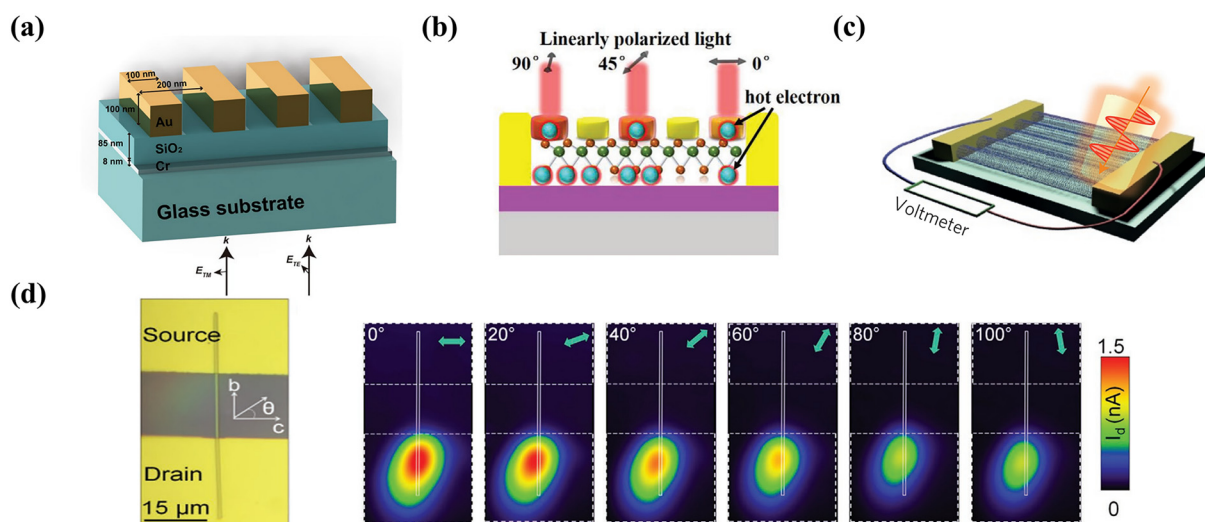
Fig. 2 Linear polarization-sensitive photodetectors based on micro–nano structures and 1D materials. (a) Structure of a broadband tunable absorber with a plasmonic grating[24] (copyright 2018, Springer Nature). (b) The schematic structure of the Au−MoS$_2$ polarization-sensitive photodetectors[25] (copyright 2020, John Wiley and Sons). (c) Schematic diagram showing the photodetector device fabricated from an aligned CNT film[26] (copyright 2016, Springer Nature). (d) Photocurrent mapping measurement of the Au/Sb$_2$S$_3$/Au photodetector[31] (copyright 2020, John Wiley and Sons).

precise fabrication and alignment of micro- and nano-structures, which are very sensitive to the aspect ratio of the device.

2.1.2 Polarization-sensitive photodetectors based on 1D semiconductor materials. 1D semiconductor materials, such as nanowires and nanotubes, characterized by distinct lattice orientations and anisotropic structures, are increasingly utilized in miniaturized polarization-sensitive photodetectors. He et al. introduced a new method for preparing large-area single-domain thin films of single-walled carbon nanotubes (SWCNTs).[26] This innovative approach is suitable for nanotubes synthesized by various methods and it affords the ability to modulate the film's thickness across a spectrum ranging from a few nanometers to approximately 100 nanometers. These films exhibit excellent optical anisotropy, characterized by significant disparities in light absorption and transmission based on the polarization direction. Specifically, these films are transparent to polarized light parallel to the nanotube alignment direction and opaque to polarized light perpendicular to the alignment direction (Fig. 2c). This unique characteristic makes them ideal polarizers in the terahertz frequency range. Furthermore, He et al. reported a carbon nanotube terahertz photodetector that operates at room temperature without an external power supply. This device is flexible and exhibits high polarization sensitivity, with a polarized ratio as high as about 5.[27]

Likewise, 1D nanowires like ZnO, GaSb, and SnO$_2$ are widely utilized in polarization-sensitive photodetection applications.[28–30] For instance, high-quality Sb$_2$S$_3$ nanowires were synthesized by Zhao et al., who systematically investigated the optical, vibrational and photoelectron anisotropy of Sb$_2$S$_3$ nanowires (Fig. 2d).[31] The photodetector based on a single Sb$_2$S$_3$ nanowire exhibits excellent polarization sensitivity in the broadband range from ultraviolet to near-infrared (360–1550 nm), and the maximum dichroism ratio reaches 2.54 (at 638 nm), achieving excellent linearly polarized photodetection. Nevertheless, the selection of 1D materials available for the fabrication of linearly polarized photodetectors is considerably limited, which is also detrimental to the future development of large-area arrays. This restricts the enhancement of photodetector performance and the expansion of their application range.

2.1.3 Polarization-sensitive photodetectors based on 2D semiconductor materials. Fortunately, since the discovery of graphene in 2004, 2D materials have also set off a wave of research. The anisotropy in 2D materials arises from the low symmetry of their crystal lattices, which imparts direction-dependent variations in electronic, optical, thermoelectric, and mechanical properties. This characteristic is instrumental for applications in electronic and optoelectronic devices, particularly in polarization-sensitive photodetectors. In theory, most of the anisotropic 2D layered materials can be divided into orthogonal, monoclinic and triclinic symmetries.[32,33] Among them, black phosphorus (BP) features an orthogonal structure with phosphorus atoms covalently linked to form a corrugated hexagonal lattice.[34] Group IV monochalcogenides like GeSe, SnS, SnSe, and SiP exhibit orthorhombic crystal

systems,[15,35–37] while GeAs, GeP, and SiAs adopt monoclinic structures.[38–40] ReS$_2$ and ReSe$_2$ are triclinic, possessing low-symmetry structures that confer significant anisotropic properties, leading to distinct in-plane optical and electrical anisotropy.[41,42]

Fig. 3 summarizes some single 2D materials with anisotropic characteristics and superior performance. Xia et al. verified the anisotropy of crystal structure, carrier mobility, conductivity, light absorption and Raman scattering of BP (Fig. 3a).[34] These anisotropic characteristics make BP provide new possibilities in the design of new optoelectronics and electronic devices, which is of great significance for promoting technological progress in related fields. However, the instability of BP in the air limits its further development, and researchers are still actively exploring better materials to replace it.[34,43–45] For example, Zhang's group investigated the atomic configuration of ReSe$_2$ nanosheets (Fig. 3b), utilizing angle-resolved Raman spectroscopy.[42] They developed photodetectors with tunable bipolar polarization sensitivity based on highly anisotropic ReSe$_2$ nanosheets with an obvious anisotropic optical response, demonstrating the polarization photodetection ability of ReSe$_2$ nanosheets for linear light.[41] ReS$_2$, which has a crystal structure similar to that of ReSe$_2$, has also been confirmed by Liu et al. to possess anisotropic properties and polarization detection capabilities. Additionally, GeSe (Fig. 3c),[15] GeP (Fig. 3d),[39] γ-InSe (Fig. 3e),[46] and GeAs$_2$ (Fig. 3f)[47] have all been confirmed to exhibit anisotropic and polarization characteristics. These 2D materials, which demonstrate in-plane anisotropy, offer significant competitive value in the field of polarization-sensitive photodetectors.

2.1.4 Improvement of polarization-sensitive photodetectors. In the field of photodetectors, high sensitivity photodetection of linearly polarized light is an important direction. However, individual materials often struggle to provide sufficient polarization sensitivity to meet the needs of high-performance photodetectors. To overcome this challenge, researchers employed a variety of strategies, including surface plasmon resonance, energy-band engineering, and gate-tunable and ferroelectric-tunable manipulation, to significantly improve the performance of polarization-sensitive photodetection.

By constructing heterostructures and using a built-in electric field to separate photogenerated carriers, the anisotropy of photocurrent can be improved, thereby enhancing polarization sensitivity. In Fig. 4a, An et al. reported a high-performance self-powered polarization-sensitive imaging photodetector based on a fully depleted van der Waals heterostructure (top-MoSe$_2$/GeSe/bottom-MoSe$_2$).[48] The full depletion of the intermediate layer GeSe significantly improves the separation efficiency and transmission speed of photogenerated carriers and achieves an excellent polarized ratio of up to 12.5, which is 3.5 times and 7 times that of MoSe$_2$/GeSe and single GeSe polarized photodetectors, respectively. This method (energy-band engineering) is also the most commonly used to enhance the performance of polarization-sensitive photodetectors.[4,17,49,50]
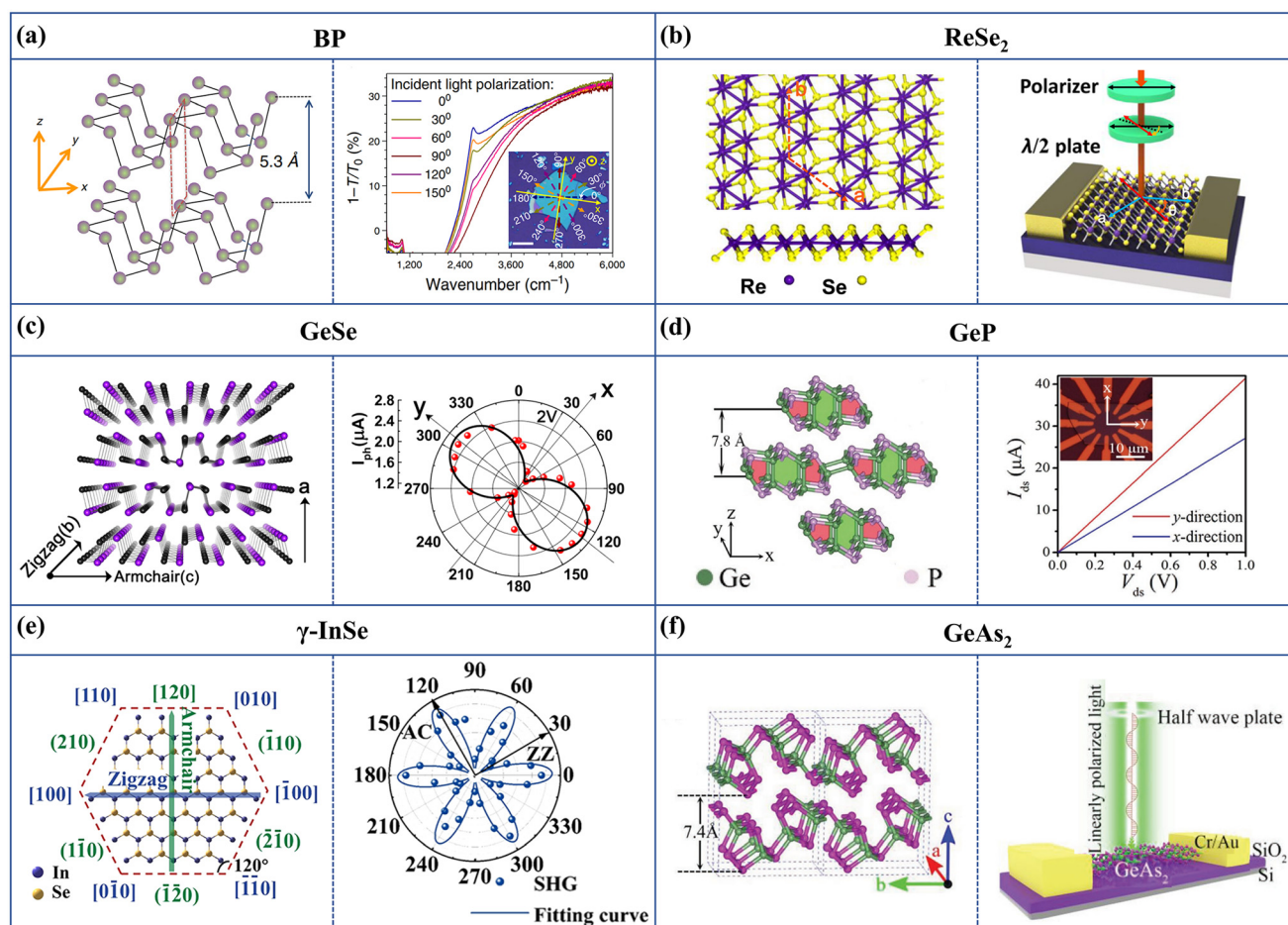
Fig. 3 2D materials with anisotropy and linear polarization-sensitive photodetectors based on these materials. (a) Characterization of the thickness of black phosphorus and polarization-resolved infrared relative extinction spectra when light is polarized along the six directions[34] (copyright 2014, Springer Nature). (b) Diagram of the crystal structure of $ReSe_2$ and polarization-sensitive photodetectors based on $ReSe_2$ nanosheets[42] (copyright 2016, American Chemical Society). (c) Atomic structure of bulk GeSe from the side view and evolution of photocurrent plotted with probe polarization from 0° to 360° at $V_d = 2$ V (ref. 15) (copyright 2017, American Chemical Society). (d) Perspective view of few-layer GeP with a single layer and typical output curves along x- and y-directions under illumination[39] (copyright 2018, John Wiley and Sons). (e) Top view of the γ-InSe nanosheet crystal structure and ARPRS and polarization-dependent SHG of the γ-InSe nanosheet[46] (copyright 2022, American Chemical Society). (f) Perspective view of few-layer $GeAs_2$ and schematic representation of the $GeAs_2$ polarization-sensitive photodetector[47] (copyright 2018, John Wiley and Sons).

Another measure to improve the performance of the polarized photodetector is to control the gate voltage. A novel photodetector based on semimetallic 1T′-MoTe₂ and the ambipolar semiconductor WSe₂ with excellent polarization sensitivity and gate-tunable optoelectronic reverse characteristics was introduced by Wang *et al.* (Fig. 4b).[51] The photodetector is capable of capturing high-resolution imaging in complex environments, with a polarized ratio that can approximately reach 30. By changing the polarized angle of the incident light, the sign reversal of the polarized photocurrent can also be observed, which allows for a possible dynamic range of polarized ratios from 1 to +∞ and from −∞ to −1.

In addition, by finely adjusting the polarization state of ferroelectric materials, the electronic properties of low-dimensional van der Waals materials can be optimized to achieve directional improvement of polarized photodetection perform-

ance. As shown in Fig. 4c, Chen *et al.* proposed a new type of van der Waals heterojunction device,[52] which relies on ferroelectric polarization control technology, by integrating a vertical heterojunction composed of GeSe and MoS₂ and a ferroelectric polymer based on P(VDF-TrFE).

Another method involves tuning the resonance frequency of surface plasmons through metal nanostructures, thereby regulating the polarization characteristics of light. Venuthurumilli *et al.* introduced an alternative method to enhance polarization sensitivity by employing two plasmonic structures—bowtie antennas and bowtie apertures—to improve the optical response of BP-based photodetectors (Fig. 4d).[53] The bowtie antenna leverages localized surface plasmon resonance to boost light absorption, predominantly in the armchair direction where absorption is more pronounced. The bowtie aperture structure, on the other hand, is designed to increase the
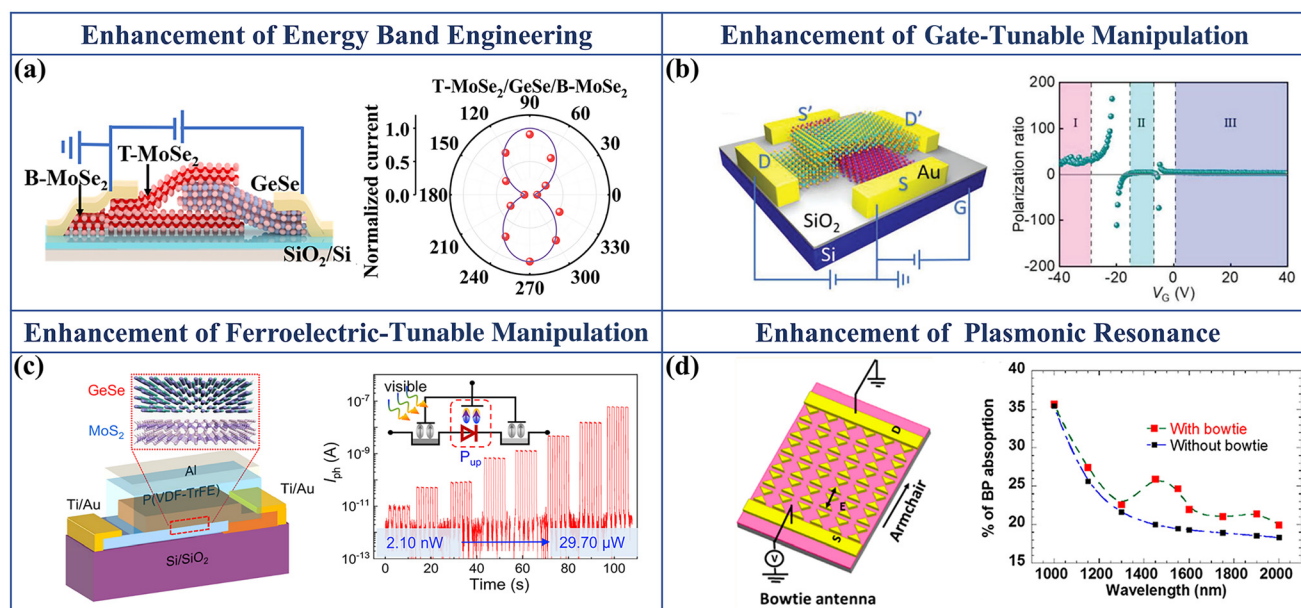
Fig. 4 Structures to improve the performance of linear polarization-sensitive photodetectors. (a) Schematic diagram of the T-MoSe$_2$/GeSe/B-MoSe$_2$ van der Waals heterostructure device, along with the polarization sensitivity characterization of T-MoSe$_2$/GeSe/B-MoSe$_2$ photodetectors[48] (copyright 2024, John Wiley and Sons). (b) Schematic diagram of the 1T'-MoTe$_2$/WSe$_2$ photovoltaic detector and calculated PR values as a function of gate voltage[51] (copyright 2023, John Wiley and Sons). (c) Schematic illustration of the GeSe/MoS$_2$ heterojunction with the P(VDF-TrFE) gate and photoresponse performance of the P(VDF-TrFE)-GeSe/MoS$_2$ heterojunction in the visible region[52] (copyright 2021, Springer Nature). (d) Schematic of a BP device with a bowtie antenna array and calculated absorption in BP, with and without bowtie structures, when illuminated along the armchair direction[53] (copyright 2018, American Chemical Society).

absorption ratio of BP to light in different polarization directions, thus enhancing polarization selectivity. These methods significantly promote the design and performance optimization of polarization-sensitive photodetectors and establish a solid theoretical and practical foundation for the future development of photodetection technology.

Linear polarization-sensitive photodetectors are crucial for polarized imaging, optical communication, and biomedical fields, but their further development is limited by technical challenges, such as the complexity of monolithic integration, cost, and alignment issues, which restrict the miniaturization and integration of the photodetectors. Moreover, although research has made progress in the integration of large-area polarization-sensitive devices, there is still a need to address the orderliness of molecular stacking structures and the consistency of orientation. Enhancing the polarized ratio of polarization-sensitive photodetectors is also a technical challenge that requires optimization of the absorption or reflection characteristics of differently polarized light through the anisotropy of materials and structural design.

2.2 Circular polarization-sensitive photodetectors

Circular polarization is a special case of elliptical polarization, where the two electric field components have a phase difference of 90 degrees and equal amplitudes.[54] Along the propagation direction, the endpoint trajectory of the electric field vector forms a circle. The electric field vector of clockwise rotation (commonly expressed as σ^+) is right-handed circularly

polarized light (RCP), and the electric field vector of counterclockwise rotation (commonly expressed as σ^-) is left-handed circularly polarized light (LCP).[55,56] The working principle of the circular polarization-sensitive photodetectors is mainly based on the difference in the absorption characteristics of the material to differently polarized light. Specifically, LCP and RCP may excite different photoelectric responses. The technology of circular polarization-sensitive photodetectors primarily relies on key mechanisms including optical chiral absorption characteristics, the circular photogalvanic effect (CPGE), the inverse spin Hall effect (ISHE), and spin-dependent recombination (SDR).[57] This chapter will elaborate on the working principles and applications of circular polarization-sensitive photodetection based on the aforementioned structures.

2.2.1 Polarization-sensitive photodetectors based on chiral characteristics. The focus of optical chiral absorption characteristics is chirality. Here, we briefly introduce what chirality is and its quantization method. The significant effect of chiral materials stems from two interactions. One is the unique interaction between different chiral molecules. Another source of research interest is the interaction of chiral materials with light, in which circular dichroism (CD) and circularly polarized luminescence (CPL) can occur.[58] CD is a chiroptical phenomenon where chiral molecules differentially absorb LCP and RCP.[59] This effect is observed within the absorption spectra of optically active compounds and is crucial for studying molecular stereochemistry and conformational changes. The distinct absorption of LCP and RCP by chiral materials leads to

changes in the transmitted light's intensity and polarization, offering insights into the molecular structure and dynamics.[60,61]

CD is usually expressed by ellipticity (Φ):[62]

$$\Phi = \frac{\pi}{\lambda(\eta_l - \eta_r)}$$

where η_l and η_r represent the absorption indices of LCP and RCP and λ represents the wavelength.

CD spectroscopy is a technique widely used to identify chiral substances based on the difference in the absorption of LCP and RCP by molecules. The CD spectra of chiral materials usually show signal peaks (positive or negative peaks) at certain wavelengths.[63] Achiral samples or racemic mixtures usually show flat spectra because there is no absorption difference for circularly polarized light.[64] When a chiral semiconductor material is used as the active layer of the photodetector, photocurrent signals of different sizes are generated due to its differential absorption of RCP and LCP, which are quantified by the dissymmetry or g-factor (denoted as g_{lum}). This factor is a key parameter for evaluating the quality of chiral materials with CPL properties.[65] In the experiment, g_{lum} can be expressed by the following formula:

$$g_{lum} = \frac{I_L - I_R}{\frac{1}{2}(I_L + I_R)}$$

where I_L and I_R denote the intensities of left-handed and right-handed CPL, respectively.

Metamaterials, a collection of 3D periodic sub-wavelength unit structures, significantly enhance the ability to control light waves, making it possible to achieve precise modulation of light waves in a changing environment. These materials can finely manipulate the phase, amplitude and polarization of light waves at the sub-wavelength scale. A metasurface, as a 2D derivative of metamaterials, is an artificial micro–nano structure. Through sub-wavelength phase control, it can accurately control the propagation of light waves and achieve comprehensive polarization analysis. Compared with the electromagnetic wave control ability of metamaterials in 3D space, metasurfaces achieve fine control of electromagnetic waves in a 2D plane.[57,66] Similar to linear polarization-sensitive photodetectors, early circular polarization-sensitive photodetectors are often based on the combination of chiral metasurfaces and photodetectors. Circularly polarized light can be effectively detected by using the difference in transmittance between LCP and RCP. Wei Li *et al.* proposed an ultra-compact circular polarization-sensitive photodetector based on chiral plasmonic metamaterials and hot electron injection.[67] The structure is shown in Fig. 5a. They achieve a circular dichroism ratio of up to 0.72 by adjusting the size and angle of the metasurface array elements. Although chiral optical effects can be reproduced by combining metasurfaces or optical elements (such as quarter-wave plates), optical elements reduce efficiency and metasurfaces increase the complexity of the system and often increase costs.[68] With the vigorous development of the field of

chiral materials, researchers are increasingly aware of their potential for effective detection of circularly polarized light.

Chirality refers to the property that an object cannot completely coincide with its mirror image, which is a key feature of these materials, including small molecules, polymers, organic crystals and perovskites.[69,70] Chiral materials can not only adapt to a variety of nanostructures (structures including 0D hybridization, 1D nanowires, and 2D films), but also meet specific application requirements.[6] Moreover, the absorption coefficients of RCP and LCP are inherently different, and the effective detection of circularly polarized light can be realized by utilizing this absorption difference. Ying Yang *et al.* used a helicene—a helically shaped chiral semiconducting molecule[71]—whose chiral structure causes a difference of about one order of magnitude in the absorption coefficients for RCP and LCP to prepare a circularly polarization-sensitive photodetector that utilizes chiral organic field-effect transistors (Fig. 5b). The transistor is highly sensitive to circularly polarized light and can detect even weak light signals effectively. It features a fast response time to light and an adjustable optical band gap, which is highly valuable for applications requiring high-sensitivity photodetection.

With the progress in the field of chiral materials, it has become a productive direction to explore the interaction between a helical structure and a π-conjugated structure. Not only are these structural extensions interconnected at multiple levels, but they also determine the chiral optical and electronic properties of the material. The periodicity and directionality of the helical structure can influence the transport and recombination of electrons within the π-conjugated system, thereby altering the material's absorption and emission properties with respect to circularly polarized light. This relationship between structural and electronic properties offers a theoretical foundation for designing molecules and materials with targeted chiral responses. The helical structure can enhance the chirality of the molecule, and the extension of the π-conjugated structure can further amplify and transfer this chirality. For example, Liu *et al.* developed a new type of double π-helical chiral molecular system fusing a perylene diimide unit (PDI) with a cyclooctatetraene unit (COT).[72] They found that with the extension of the length of the chiral helical chain, the chiral optical properties were significantly enhanced, indicating that the combination of the helical structure and the π-conjugated structure played an important role in chiral transfer and amplification (Fig. 5c). A. Ishii *et al.* constructed a 1D perovskite structure by incorporating chiral cations (NEA$^+$) that influence the helicity of the $(PbI_6)^{4-}$ chains in the perovskite.[73] This structure exhibits a strong CD signal of more than 3000 mdeg due to its spiral shape, with a high anisotropy factor of 0.04. The CPL detector utilizing this 1D perovskite structure successfully achieved an exceptional polarized discrimination ratio of 25.4.

In addition, by integrating chiral molecules into perovskite structures, the inherent chirality of these molecules can be used to enhance the sensitivity of materials to circularly polarized light, which is an important supplement
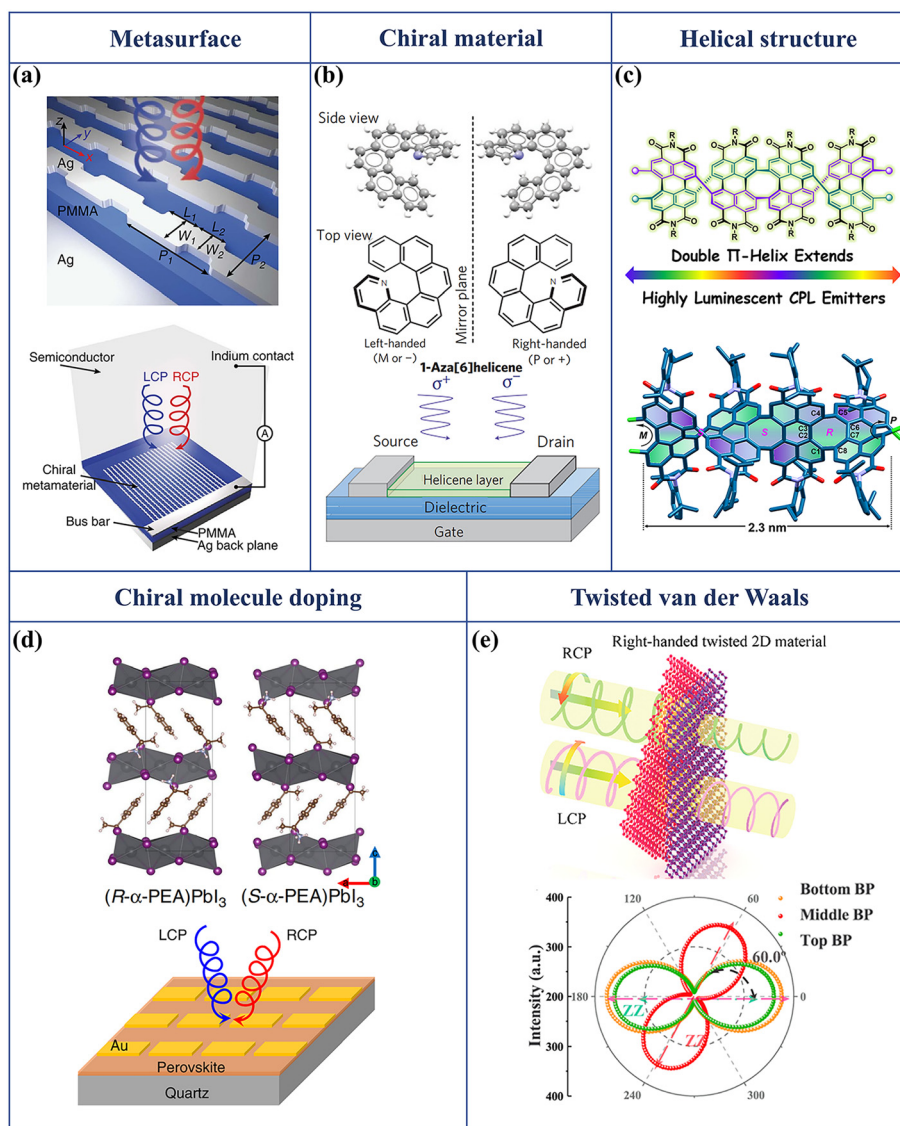
Fig. 5 Circular polarization-sensitive photodetectors based on chiral characteristics. (a) Schematic of the chiral metamaterial and the CPL photo-detector[67] (copyright 2015, Springer Nature). (b) Molecular structure and device architecture of the circularly polarized photo-detecting helicene OFETs[71] (copyright 2013, Springer Nature). (c) Highly luminescent CPL emitters featuring a double T-helix extension and single-crystal structures of rac-5[72] (copyright 2024, American Chemical Society). (d) The crystal structures of our chiral perovskites and the device structure of the (R- and S-α-PEA)PbI$_3$ film photodetector[74] (copyright 2019, Springer Nature). (e) Schematic illustration of different circularly polarized lights passing through the twisted 2D material and the orientation of the top and bottom BP crystals[76] (copyright 2023, American Chemical Society).

to traditional inorganic semiconductor materials. The Chen group introduced a hybrid perovskite, (α-PEA) PbI$_3$, integrating chiral α-phenylethylamine (α-PEA) with lead iodide (PbI$_3$)[74] (Fig. 5d). This material synergizes the CPL-sensitive absorption of chiral organics with the charge transport efficiency of inorganics.

In addition to the above materials and structures, 2D materials with chiral structures can also serve as ideal materials for chiral optoelectronic devices. Niu *et al.* explored how chirality affects 2D tellurium's (Te) response to circularly polarized light in field-effect transistors.[75] They found that both the longitudinal circular photogalvanic effect (CPGE) and

the circular photovoltaic effect (CPVE) depend on Te's chiral crystal structure. These effects make 2D Te a promising material for chirality-dependent optoelectronics. The study also shows that by adjusting the back-gate voltage, one can control the chiral properties and photocurrent response in 2D Te. In Fig. 5e, Wang *et al.* demonstrated that the chirality of these materials can be significantly adjusted by varying the twist angle between layers.[76] This tunability, influenced by an-isotropy and band structure, extends across the visible to infra-red spectrum. The potential for spin-selective information transformation highlights their promise in spintronics, polar-ization optics, and nano-optoelectronics.

2.2.2 Polarization-sensitive photodetectors based on the circular photogalvanic effect (CPGE). The second method for achieving circular polarization photodetection capability leverages the spin-photoelectric effect, a phenomenon that arises from the intricate interplay between light and electron spins within materials. A notable aspect of this field is the circular photogalvanic effect (CPGE), which occurs upon the incidence of circularly polarized light.[77] The photocurrent induced by the CPGE is sensitive to the polarization axis of the incident light and is considered a nonlinear photoelectric response. The origins of the CPGE are intricately linked to electron spin, valley degree of freedom, material symmetry, and the Berry phase, offering a novel avenue for probing the fundamental physical properties of materials.[78,79] This effect not only enhances our understanding of spin optoelectronics but also paves the way for developing advanced circular polarization-sensitive photodetectors.

Significant progress has been made in elucidating the CPGE, especially in understanding the basic mechanism of photoexcited spin current. For example, in semiconductor heterostructures, the spin–orbit interaction associated with the Rashba effect drives the CPGE, while in topological Weyl semimetals, the interplay between the Berry phase and the Pauli blocking effect governs the selection of electron momentum. In 2D transition metal dichalcogenides (TMDCs), the valley

polarization currents are excited by circularly polarized light.[75,77,80–82] These insights not only enhance our understanding of the CPGE, but also pave the way for innovative electronic device architectures based on spin and valley degrees of freedom. Duan *et al.* realized the Berry curvature dipole (BCD) generated on the asymmetric heterogeneous interface of semiconductors and its application in helicity-to-spin conversion.[83] They formed a WSe_2/SiP (Fig. 6a) heterogeneous interface by stacking van der Waals monolayer materials with different lattice symmetries, breaking the rotational symmetry in the material, realizing the symmetry breaking of the interface crystal structure and the artificial modification of the energy band structure, and using their symmetry mismatch to induce the BCD. By changing the energy of the incident light and the gate voltage, the spin photocurrent at the heterogeneous interface can be regulated. The non-linear effect of Weyl semimetals is a unique phenomenon in topological materials. Ma *et al.*, for the first time, observed a huge multiphoton response in type II Weyl semimetals.[84] The experimental diagram is shown in Fig. 6b. The Berry curvature divergence at the Weyl node is the key factor that causes $TaIrTe_4$ to produce a huge photocurrent response in the mid-infrared band. This divergence is similar to the magnetic monopole in the momentum space, and its sign determines the chirality. Not only is the nonlinear response of
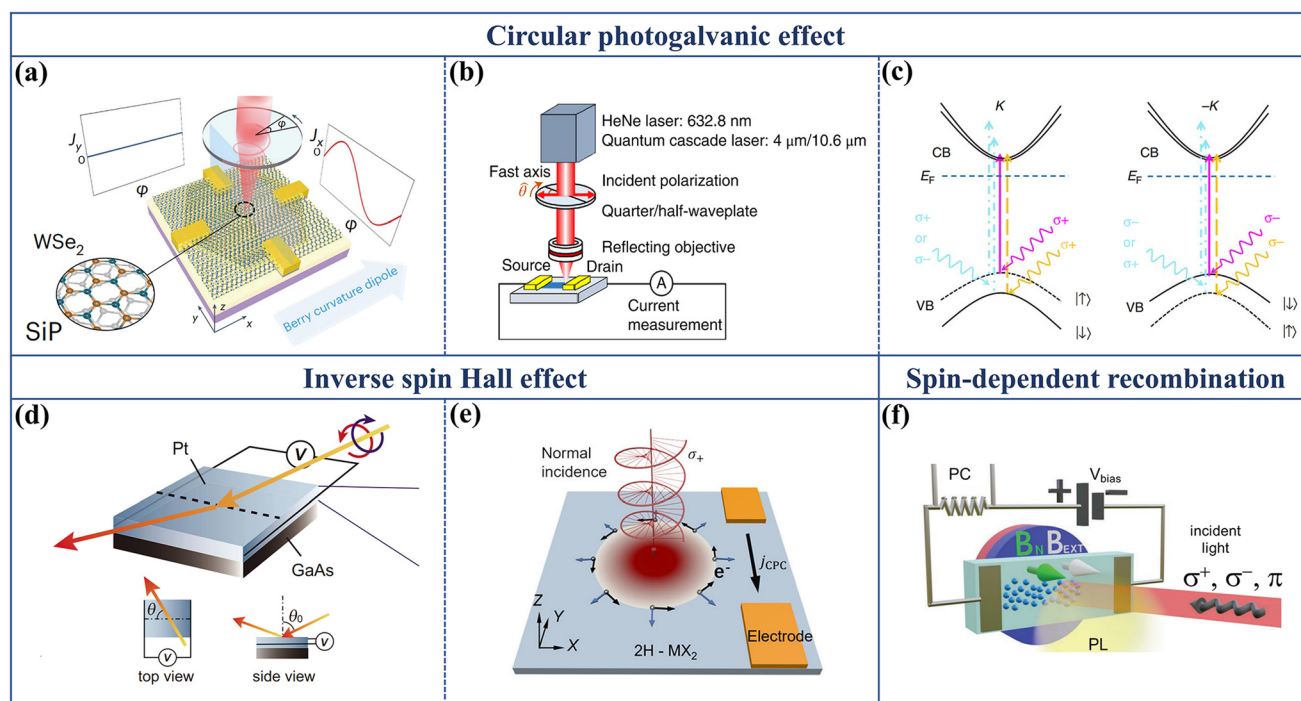

Fig. 6 Circular polarization-sensitive photodetectors based on the CPGE, ISHE and SDR. (a) Schematic figure for generation of the spin photocurrent for the WSe_2/SiP device with incident light normal to the heterointerface[83] (copyright 2023, Springer Nature). (b) Schematic diagram of the polarization-resolved scanning photocurrent measurement setup[84] (copyright 2019, Springer Nature). (c) Band diagram of K and −K valleys of MoS_2 and photocurrent generation[86] (copyright 2015, Springer Nature). (d) A schematic illustration of the Pt/GaAs hybrid structure used in this study[87] (copyright 2010, AIP Publishing). (e) Schematic diagram depicting the creation of a spin current induced by the intensity gradient of the Gaussian beam, subsequently converting into the circulating charge current[91] (copyright 2024, Springer Nature). (f) Sketch of the experimental configuration used to simultaneously measure the photoluminescence (PL) and the PC[93] (copyright 2021, John Wiley and Sons).

photocurrent observed, but the anisotropic and circularly polarized photocurrent effects are found also in different crystal directions. Moreover, Ni et al. mainly studied the longitudinal circularly polarized photocurrent effect generated by circularly polarized light excitation in chiral multi-fold half-metal CoSi.[85] Through terahertz emission spectroscopy, a huge longitudinal photocurrent of about 550 μA V^{-2} was observed at a specific energy, and it was proved to be derived from topological band crossing. In addition, in TMDs such as MoS_2, the valley polarization current generated by circularly polarized light is also an important manifestation of the CPGE. Valleytronics aims to increase the degree of freedom of optoelectronic devices by using valley degeneracy in the semiconductor energy band. Eginligil et al. found that monolayer MoS_2, as a new valley electron material, exhibits significant valley polarization characteristics in photoluminescence, as revealed in Fig. 6c.[86] By adjusting the polarized angle of the laser, they explored the correlation between the photocurrent and the polarized angle of the light, thus confirming the feasibility of controlling the spin–valley coupling current by precisely controlling the polarization of the light.

2.2.3 Polarization-sensitive photodetectors based on the inverse spin Hall effect (ISHE).

There is another effective way to explore the realization of circularly polarized photodetection capability, which involves the use of circularly polarized light-induced spin selectivity. Inside the semiconductor material, the selection rule in the light absorption process can generate electrons with specific spin orientation in the conduction band, which depends on the absorption of photons with specific polarization states. When these electrons absorb circularly polarized light, their spin states will be affected, thus realizing the conversion from the polarization state of light to the spin state of electrons. This mechanism allows the polarized information of light to be utilized in the application of spintronics.[87] The inverse spin Hall effect (ISHE) is a phenomenon at metal–semiconductor interfaces where a spin current is generated perpendicular to both the current and spin polarization directions when current passes through a material with strong spin–orbit coupling.[88] This effect is crucial for converting spin information into electrical signals in spintronics. Although the ISHE does not directly involve the conversion of light polarization into electrical signals, its role is to convert electrical signals into spin currents. This capability can be combined with the conversion of light polarization information (through other phenomena such as circularly polarized light-induced spin selectivity) to achieve a broader range of spintronic applications.[89]

K. Ando et al. used a Pt/GaAs hybrid structure for experiments (Fig. 6d).[87] Within the GaAs layer, the absorption of circularly polarized light, in line with optical selection rules, gives rise to spin-polarized electrons in the conduction band, effectively translating the circularly polarized information of light into electron spin polarization. These spin-polarized electrons are then injected into the Pt layer as a pure spin current, facilitated by the Pt/GaAs interface. The robust spin–orbit coupling inherent to Pt materials enables the conversion of

these injected pure spin currents into electric potential or electromotive force (EMF) through the ISHE. This phenomenon harnesses the spin–orbit interaction to encode spin information into electrical signals, offering a novel perspective on the design and material selection for photodetectors, which is pivotal for enhancing the efficiency of photoelectric effects. Khamari et al. presented a spin-optoelectronic detector that harnesses the ISHE in an Au/InP hybrid structure to concurrently measure the degree of circular polarization and the intensity of a laser beam.[90] This device, integrating dual detectors on a single chip, leverages the ISHE for polarization assessment and the photovoltaic effect for intensity, operating without crosstalk. It offers rapid response, compactness, and integrability, advancing photonic and optical communication applications. In centrosymmetric materials, due to the existence of global inversion symmetry, hidden spin polarization is usually difficult to convert into spin current. In the work of Wang et al.,[91] a spatially-varying circularly polarized light beam is normally incident on the centrosymmetric TMD semiconductor without an applied electric field. The spatial variation of the beam breaks the inversion symmetry of the system, as illustrated in Fig. 6e. By altering the electrode configuration, illumination position, and spot size, spin-polarized circularly polarized photocurrent was observed in multilayer 2H-MoTe$_2$, 2H-MoS$_2$, and 2H-WSe$_2$.

2.2.4 Polarization-sensitive photodetectors based on spin-dependent recombination (SDR).

The last major mechanism introduced in circular polarization-sensitive photodetectors is spin-dependent recombination (SDR). The SDR phenomenon describes the process of electron–hole recombination in semiconductor materials, which is significantly influenced by the spin states of the carriers involved in the recombination. Specifically, circularly polarized light, due to its specific spin angular momentum, can interact with the spin states of electrons in semiconductors, thereby achieving control over the spin states.[92,93] This characteristic of light–matter interaction provides the physical foundation for realizing circular polarization-sensitive photodetection.

Among them, GaAsN (this is a class of semiconductors based on GaAs, with a small amount of nitrogen (N) elements incorporated), due to its unique band structure, shows significant advantages in photodetector applications.[93] The introduction of GaAsN materials can significantly enhance the sensitivity of photodetectors to circularly polarized light, which is difficult to achieve with traditional non-chiral III–V or IV–VI semiconductor materials. The performance enhancement achieved by GaAsN is mainly attributed to its spin-dependent recombination mechanism. This mechanism allows GaAsN materials to electrically measure the polarization state of light at room temperature, which not only simplifies the complexity of the system but also promotes the miniaturization and integration development of photodetectors.[94,95] In Fig. 6f, Joshya et al. fabricated a GaAsN-based chiral photodetector capable of determining light polarization and intensity through conductivity measurements.[93] They leveraged the chiral photoconductivity effect of the GaAsN epitaxial layer, which is influenced by

spin-dependent recombination and spin-polarized defects. The researchers demonstrated that by manipulating the spin polarization of conduction band electrons, the material's conductivity could be controlled. Furthermore, they showed that applying an external magnetic field could adjust the hyperfine interaction and the Zeeman effect, thereby modulating the material's response to circularly polarized light (RCP or LCP). Ibarra-Sierra *et al.* prepared a novel spin-optoelectronic device that translates light's polarization into electrical signals *via* spin-dependent recombination and hyperfine interaction.[96] In $GaAs_{1-x}N_x$, spin-polarized electrons and holes, excited by circularly polarized light, interact with Ga^{2+} centers, prolonging the lifetime of electrons with certain spin orientations while rapidly recombining others. This results in a buildup of spin-polarized electrons. The hyperfine interaction with the Ga^{2+} center's bound electrons and nucleus produces an Overhauser-like field under an external magnetic field, which differentially responds to the chirality of circularly polarized light, allowing the device to identify the light's chirality.

The development of circular polarization-sensitive photodetectors has been facilitated by a profound understanding of the physical mechanisms of optical absorption, CPGE, ISHE, and SDR. These technological breakthroughs have not only enhanced the performance and sensitivity of the photodetectors but also expanded their application prospects in fields such as optical imaging, optical communication, and quantum information processing. Despite facing technical challenges such as material property limitations, weak photocurrent, fabrication difficulties, and lattice mismatch issues, future development directions will focus on the development of new chiral semiconductor materials, exploration of new photoelectric mechanisms that directly respond to the spin of photons, optimization of artificial nanostructures, and the development of heterojunction devices, aiming to achieve higher-performance direct detection of circularly polarized light and broader applications.

2.3 Full-Stokes polarization-sensitive photodetectors

Full-Stokes polarization is an analytical method used to describe the polarization state of light by using Stokes parameters, which enables complete characterization of the polarization characteristics of any polarized light.[19,20,97] The Stokes parameters are a set of four scalar values,[19,98] which can be expressed as $S = (S_0, S_1, S_2, S_3)^T$

$$\text{These parameters can be defined as :}\begin{cases} S_0 = I \\ S_1 = I_{0°} - I_{90°} \\ S_2 = I_{45°} - I_{-45°} \\ S_3 = I_{RCP} - I_{LCP} \end{cases}$$

Here, the parameter S_0 represents the total intensity of the light wave, summing intensities across all polarization directions, and is a scalar indicating the light wave's total energy independent of the polarization direction. S_1 denotes the intensity difference between horizontally and vertically polarized light components. A positive S_1 indicates stronger horizontal polarization, a negative suggests stronger vertical polar-

ization, and zero implies equal intensities, suggesting non-polarized or circularly polarized light. S_2 describes the intensity difference between light polarized at +45° and −45°. A positive S_2 indicates stronger +45° polarization, a negative suggests stronger −45° polarization, and zero indicates equal intensities in both directions. S_3 represents the intensity difference between RCP and LCP. A positive S_3 indicates stronger right-handed polarization, a negative indicates stronger left-handed polarization, and zero signifies the absence of circular polarization or equal intensities of both components. Through the description of the unit vector, all possible polarization states can be geometrically expressed as a point on the unit ball, which is called the Poincaré sphere. Its three coordinate axes correspond to the three parameters of S_1, S_2, and S_3, respectively. The surface of the ball can represent all fully polarized light, and the interior of the ball represents incompletely polarized light, while natural light is at the origin.

The Stokes vector is composed of four parameters, which provide a theoretical basis for the comprehensive characterization of polarized light. It delineates various polarized modes, including linear, circular, and their complex combinations, with detailed precision.[19,99] Accurate measurement of these parameters allows for a detailed quantitative analysis of polarized light, revealing the underlying physical mechanisms. Developing photonic materials that are highly sensitive to both linear and circular polarization is crucial for constructing high-performance Stokes photodetectors. Such materials are essential for the accurate detection of polarized light. The full-Stokes polarization measurement technology, as an advanced analytical tool, significantly enhances our understanding of subtle differences in polarized light characteristics. It offers a comprehensive analysis of the polarization state and elucidates the polarization effects during light–matter interactions, providing valuable information for polarization research.

2.3.1 Polarization-sensitive photodetectors based on metamaterials and metasurfaces. The development of full-Stokes polarization-sensitive photodetectors has undergone several pivotal stages. A traditional approach involves integrating a phase extraction layer with linear polarization-sensitive photodetectors to capture circularly polarized data.[100,101] This enhancement allows for the reconstruction of the complete polarization state of the incident light, including both linear and circular components. However, it may escalate photodetector complexity and costs, and the additional extraction layer could reduce light transmission efficiency. By employing advanced metamaterials and metasurface technologies, photodetectors that can simultaneously extract linearly polarized and circularly polarized light components can be designed. Subsequently, the Stokes parameters of the incident light can be further calculated from the photocurrent information captured by the photodetector, thus providing a comprehensive description of the polarization characteristics of the light.[102]

In the early stages of technological development, photodetectors mainly rely on traditional time-resolved measurement techniques. In order to capture the complete polarization state of light, at least four independent measurements
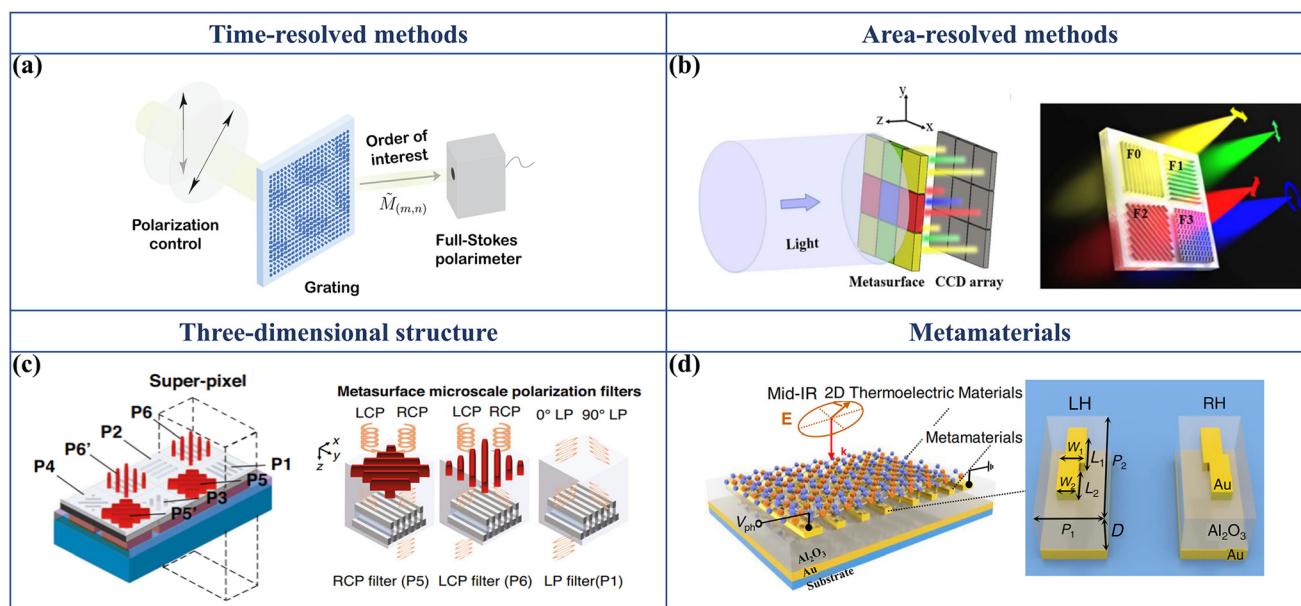
Fig. 7 Full-Stokes polarization-sensitive photodetectors based on metamaterials and metasurfaces. (a) Matrix gratings for arbitrary parallel polarization analysis[103] (copyright 2019, The American Association for the Advancement of Science). (b) Schematic of the setup for near-infrared full-Stokes photodetection[104] (copyright 2021, Optica Publishing Group). (c) CMOS integrated full-Stokes polarimetric imager with dual operation wavelengths[102] (copyright 2023, Springer Nature). (d) Design architecture of a full-Stokes photodetector based on chiral plasmonic metamaterials[57] (copyright 2022, Springer Nature).

are needed to determine the Stokes parameters of incident light. Rubin *et al.* from Harvard University developed a novel sub-wavelength diffraction grating for precise polarization control at visible frequencies.[103] The grating, depicted in Fig. 7a, consists of anisotropic nanostructures that enable dynamic light polarization. By coupling with an imaging lens and sensor, it captures four diffraction orders, each filtered by different polarizers on the metasurface. A pixel-wise analysis of these images allows for the reconstruction of the four Stokes parameters of the scene. However, the method's reliance on time-sharing technology limits its speed, making it unsuitable for real-time polarization analysis of dynamic scenes. Then, different from the above time-resolved measurement, Zhang *et al.* have developed a pixel-based metasurface on an insulating silicon wafer for full-Stokes vector polarized photodetection in the near-infrared spectrum (Fig. 7b).[104] The design integrates a 'Z'-shaped circular polarizer with three linear polarizers, enabling simultaneous photodetection of linear and circular polarization states. This approach is compatible with semiconductor manufacturing, advancing on-chip polarized photodetection and polarized imaging technology. In addition, as illustrated in Fig. 7c, Zuo *et al.* have introduced a biomimetic full-Stokes polarized imaging sensor utilizing metasurface on-chip integration.[102] A layer of a silicon metasurface that produces optical birefringence is stacked with a layer of a high-performance linearly polarized photodetection metasurface to achieve high-performance circularly polarized photodetection. Notably, the polarized extinction ratio of the biomimetic circular polarizer shows insensitivity to the incident angle, which ensures the high-precision polarized

measurement capability of the sensor in a large field of view. This metasurface-based technology excels in imaging speed, integration, accuracy, and compatibility with standard semiconductor processes, providing a promising direction for future optical imaging advancements.

In addition, researchers have discovered that it is possible to use metamaterials to achieve full-Stokes polarization-sensitive photodetection. Dai *et al.* have developed a novel on-chip mid-infrared photodetector for full-Stokes polarization photodetection (Fig. 7d).[57] This design employs chiral plasmonic metamaterials to selectively absorb light with specific polarizations, converting this absorption into electrical signals through the photoelectric thermoelectric effect. The polarization sensitivity is tunable by adjusting the chiral metamaterials' spatial and geometric attributes, enabling the photodetection of both linear and circular polarization. The presented compact chip design is conducive to integrated polarized measurements in miniaturized optoelectronic systems. The photodetector's operation is not limited by the band gap of its active material, enhancing its application potential in different wavelength regions.

The ongoing interest in metamaterials and metasurfaces is expanding, particularly for their potential in creating compact, full-Stokes polarization-sensitive photodetectors that are easily integrated into smaller systems, aligning with the demand for miniaturization in modern optical devices.[13,14,105] As on-chip integrated photodetector technology advances, simplifying the manufacturing process and achieving miniaturization of these photodetectors are crucial. Researchers are now leveraging the intrinsic properties and chiral control of low-dimensional
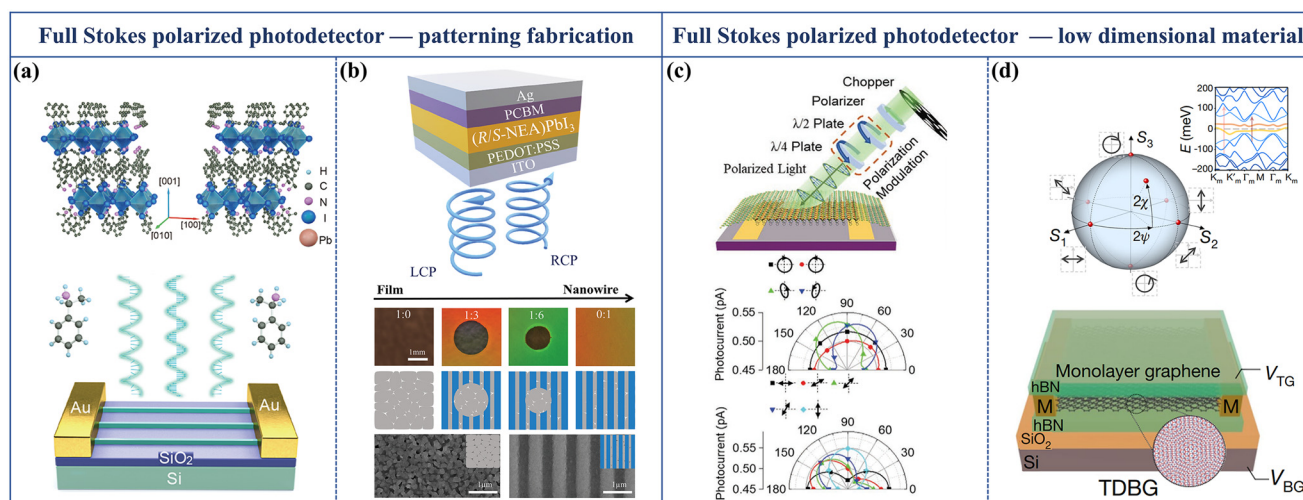
Fig. 8 Full-Stokes polarization-sensitive photodetectors based on low-dimensional materials. (a) Crystal structure and device architecture of a Stokes-parameter photodetector[106] (copyright 2021, American Chemical Society). (b) Schematic diagram of a chiral perovskite-based photodetector and schematic diagrams of perovskite films with different imprinted area ratios[109] (copyright 2024, John Wiley and Sons). (c) Full-Stokes polarimetric measurements and schematic of the setup for the polarization-resolved photocurrent measurement[107] (copyright 2021, John Wiley and Sons). (d) Polarization states of incident light, described by Stokes parameters and drawn on the Poincaré sphere and schematic of the TDBG photodetector[111] (copyright 2022, Springer Nature).

materials for full-Stokes photodetection, marking a significant shift from metamaterial-based to low-dimensional material-based photodetectors and offering a new pathway to enhance photodetection performance.[106–108]

2.3.2 Polarization-sensitive photodetectors based on low-dimensional materials. Low-dimensional materials, owing to their unique properties, are typically more suitable for use in high-integration full-Stokes photodetectors. First, in the latest development of polarized photodetection technology, low-dimensional materials are processed using the patterning fabrication method, which has attracted wide attention in the preparation of full-Stokes polarization-sensitive photodetectors. By inserting chiral cations between the perovskite layers, Zhao et al. realized the controlled synthesis of chiral 2D perovskite nanowires and prepared a full-Stokes photodetector based on chiral 2D perovskite nanowire arrays (Fig. 8a).[106] The interlayer chiral cations facilitate the photodetection of circularly polarized light, with a maximum anisotropy factor of 0.15. Additionally, the nanowires, characterized by an anisotropic dielectric function, enable the photodetection of linearly polarized light, achieving a polarized ratio of 1.6. Moreover, Wang et al. constructed a novel self-powered full-Stokes photodetector based on a patterned chiral perovskite film (Fig. 8b).[109] The optically active perovskite materials were synthesized with the incorporation of chiral molecules, and nanowire array structures were engineered on the perovskite film surfaces through patterning techniques to enhance sensitivity towards linearly polarized light. By modulating the ratio of the patterned nanowire array to the circular region, the photodetector's balance of response to circularly polarized light and linearly polarized light can be dynamically adjusted, achieving a circular polarization sensitivity coefficient of up to 0.125 and

a linear polarization ratio of 1.5. Consequently, the photodetector is capable of effectively discerning two polarization states of light simultaneously. By patterning preparation and using the synergistic effect of linear and circular polarization responses, the measurement of full-Stokes parameters is achieved, which provides a new way for polarized photodetection and imaging of high-performance Stokes parameter photodetectors.

In addition, the full-Stokes polarization-sensitive photodetectors prepared with low-dimensional materials can directly use the intrinsic characteristics of the material to perceive the polarized light, which is more conducive to achieving highly integrated devices and reducing production costs. It is an important research direction for the future development of full-Stokes polarized photodetectors. First, as shown in Fig. 8c, this review reports a full-Stokes polarimeter based on chiral perovskite materials, which can fully analyze the polarization state of light.[107] The authors successfully constructed an integrated full-Stokes polarimeter using the optical anisotropy and response characteristics to circularly polarized light of chiral 2D perovskite materials (S- and R-MBA)$_2$PbI$_4$ (MBA = C$_6$H$_5$C$_2$H$_4$NH$_3$). The device can accurately distinguish various types of polarized light, including linearly polarized light and circularly polarized light, without additional filters. Similar phenomena were also observed by Zhao et al., who recently constructed an innovative full-Stokes polarized photodetector with chiral 2D/quasi-2D perovskite heterojunction nanowire arrays.[110] The work skillfully constructed a built-in electric field and utilized the anisotropy of the material to achieve high sensitivity photodetection of circularly polarized and linearly polarized light.

Moreover, similar to the previous circular polarization-sensitive photodetectors in this review, 2D materials can achieve

polarized photodetection with different capabilities through twisted layers. Ma *et al.* employed the tunable mid-infrared bulk photovoltaic effect (BPVE) in twisted bilayer graphene (TDBG) combined with a convolutional neural network (CNN) to achieve full-Stokes polarimetry (Fig. 8d).[111] The photovoltage mappings (V_{ph}) produced by the TDBG device encode the polarization state and wavelength of incident light. Through training, the CNN can parse these mappings to extract the complete Stokes parameters and incident light wavelength from a single device. This capability enables simultaneous polarization and wavelength photodetection, essential for comprehensive full-Stokes analysis.

Full-Stokes polarization-sensitive photodetectors are evolving towards greater integration, real-time capabilities, and high sensitivity, enabling a comprehensive description of the polarization state of light and finding broad applications in fields such as autonomous driving and machine vision. Currently, these photodetectors face challenges including manufacturing complexity and measurement accuracy issues. Future research will focus on improving the measurement speed, wavelength compatibility, and reducing costs and size for better integration into existing systems. Additionally, the application of new materials and low-dimensional materials will pave new ways to enhance polarization-sensitive photodetection performance.

3. Summary and outlook

In this review, a comprehensive history and recent advances in linear, circular, and full-Stokes polarization-sensitive photodetectors are demonstrated. Table 1 summarizes the parameters and performance indicators of these three kinds of photodetectors. Obviously, as appealing platforms, several asymmetric or chiral nanostructured materials with a number of intriguing nonlinear photoelectric properties have established themselves as versatile building blocks in novel monolithic integration polarization-sensitive photodetectors. These materials not only enhance the performance of the photodetectors through alterations in their crystal structure and geometry but also enable the monitoring of multidimensional information, including light intensity, wavelength, polarization, phase, and even angular momentum, by modulating the anisotropy of the nanomaterials. Notably, full-Stokes polarimetry can be achieved using surface plasmon resonance metasurfaces, further expanding the capabilities of these photodetectors as appealing platforms.[100,112]

In practical applications, polarization-sensitive photodetectors have been extensively utilized across various fields. Polarized imaging technology, as an advanced optical detection method, has been demonstrated to significantly enhance the capabilities of target detection and recognition in complex backgrounds. For instance, it is effective in detecting targets such as camouflaged trucks and landmines, which are difficult to identify using conventional imaging systems due to their concealment.[113] In the biomedical field, polarized imaging

aids in more precise tumor diagnosis by analyzing the differences in polarized properties between healthy and pathological tissues.[114] Moreover, as an advanced imaging technique, polarized light has been widely applied to improve the accuracy and reliability of facial recognition.[115] The use of polarized light not only enhances the resolution of thermal imaging systems but also increases their resistance to environmental interference, which is crucial for the development of modern security technologies. This technology demonstrates immense potential for application in various fields such as photography, navigation, and augmented reality and is expected to play a more critical role in future technological advancements.

However, with regard to the overall perspective, the study of polarization-sensitive photodetectors towards monolithic integration, real-time capabilities, and high sensitivity is still at its preliminary stage.

First, in order to achieve high responsivity and anisotropic ratios at specific wavelengths for polarization-sensitive photodetectors, strategies that are facile, low-cost, highly reliable, and repeatable for fabricating 1D nanostructure arrays, 2D materials, chiral materials, or their heterostructures with fewer defects at a centimeter scale should be developed. In addition, it is critical to further modify the properties of these devices by topography processing, doping and designing distinct functional structures (metasurface, moiré superlattices, *etc.*).[117–120]

Second, research on polarization-sensitive photodetectors has primarily focused on the development of individual materials up to now, and widespread integrated devices are still lacking. However, a single material cannot selectively detect the linearly/circularly polarized information of a target at the same time. Therefore, schemes of multi-material integration as well as silicon-based semiconductors are urgently needed to be developed.

Third, to transition these novel nanostructured polarization-sensitive photodetectors from the lab to practical use, the technical combination between excitation of nonlinear photoresponse and polarized photodetection is also an important issue to be considered. In particular, non-linear light–matter interactions and multiphoton nonlinear physical processes have a significant impact on the photoelectric conversion efficiency, which is promisingly modified by bandgap engineering, spin effects, the morphology of the metasurface, *etc.*

Although many thorny issues need to be solved in this burgeoning field, it is believed that opportunities grow out of challenges. Therefore, the combination of deep fundamental research and novel industrial technology will lead to more and more exciting discoveries in the next generation of polarization-sensitive photodetectors. With the continuous advancement of technology, polarized detectors will evolve towards greater diversification. The improvement of technology and performance for polarized photodetection and polarized all-optical detection is expected to break through the limitations of traditional photoelectric conversion and achieve higher sensitivity and lower power consumption. These above technologies will bring transformative changes across various fields,

Table 1 Performance of linear, circular, and full-Stokes polarization-sensitive photodetectors

	Device	Wavelength (nm)	Voltage (V)	Responsivity (mA W^{-1})	Detectivity (Jones)	Anisotropy (I_{max}/I_{min})	Ref.
Linear	MoS$_2$/Au	660	0	26 000		1.45	25
	Sb$_2$S$_3$	638	2	343.4		2.54	31
	γ-InSe	405	1	127 000	2.73 × 10^{11}	2.07	46
	ReSe$_2$	633	1				42
	GeSe	532	2	4250		1.09	15
		638	2			1.44	
		808	2			2.16	
	GeAs$_2$	532	1			2	47
	GeP	532	0.1	3110		1.83	39
	PdSe$_2$	532	1	3.5		1.9	116
	SiAs	514.5	2			5.3	40
		325	2			2.3	
	BP/plasmonics	1550	100 mV	14.2	2.91 × 10^{13}	8.7	53
	Te/MoSe$_2$	405	0	2106		16.39	17
	MoTe$_2$/WSe$_2$	635	0	212.15	4 × 10^{10}	30	51
	MoSe$_2$/GeSe/MoSe$_2$	635	0	206	6.6 × 10^{10}	12.5	48
	MLG/ReSe$_2$/SnSe$_2$	635	0	144	2.4 × 10^{10}	13.27	4

	Device	Wavelength (nm)	Voltage (V)	Responsivity (mA W^{-1})	Detectivity (Jones)	Anisotropy factor (g)/CD	Ref.
Circular	Chiral metamaterial (PMMA/Ag)	1340		2.2		CD = 0.72	67
	(R-and S-α-PEA)PbI$_3$	395	20	797	7.1 × 10^{11}	CD = 0.9	74
	BP-BP	665				Ellipticity = 1581 mdeg	76
	PDI-entwined double π-helical nanoribbons	562				g = 0.015	72
Full-Stokes	(S-α-PEA)$_2$PbI$_4$ and (R-α-PEA)$_2$PbI$_4$	505	5	47.1 × 10^3	1.24 × 10^{13}	Linear: 1.6; Circular: g = 0.15	106
	(S-and R-MBA)$_2$PbI$_4$	512	−3	136	1.2 × 10^{10}	Linear: 1.46; Circular: g_{CD} = −8 × 10^{-4}	107
	(R/S-NEA)PbI$_3$	405	0			Linear: 1.5; Circular: g = 0.125	109
	Metasurface CCD array	1.65 μm				Circular: CD = 0.7	104
	[(R)-β-MPA]$_2$PbI$_4$ and [(S)-β-MPA]$_2$PbI$_4$	510	5			Linear: 1.5; Circular: g = 0.38	110

including polarized imaging, optical communication, quantum optics and so on. Moreover, the integration of polarized detection technology with biology and medicine holds the promise of broader application breakthroughs, paving the way for innovative solutions and expanded possibilities. As a result, it means that strengthening interdisciplinary cooperation is important to promote the advancement of polarization-sensitive photodetection technology.[121–124] It is hoped that this review will inspire researchers and engineers from the fields of physics, materials science, optical engineering, and electronic engineering to collaboratively advance the development of polarization-sensitive photodetectors.

Data availability

No primary research results, software or code have been included and no new data were generated or analysed as part of this review.

Conflicts of interest

The authors declare no competing financial interest.

Acknowledgements

References

1 H. Chen, H. Liu, Z. Zhang, K. Hu and X. Fang, *Adv. Mater.*, 2016, **28**, 403–433.

2 X. Wang, Y. Wang, W. Gao, L. Song, C. Ran, Y. Chen and W. Huang, *Adv. Mater.*, 2021, **33**, 2003615.

3 C. He, H. He, J. Chang, B. Chen, H. Ma and M. J. Booth, *Light: Sci. Appl.*, 2021, **10**, 194.

4 Y. Pan, T. Zheng, F. Gao, L. Qi, W. Gao, J. Zhang, L. Li, K. An, H. Gu and H. Chen, *Small*, 2024, **20**, 2311606.

5 N. Zhou, Z. Dang, H. Li, Z. Sun, S. Deng, J. Li, X. Li, X. Bai, Y. Xie, L. Li and T. Zhai, *Small*, 2024, **20**, e2400311.

6 W. Xin, W. Zhong, Y. Shi, Y. Shi, J. Jing, T. Xu, J. Guo, W. Liu, Y. Li, Z. Liang, X. Xin, J. Cheng, W. Hu, H. Xu and Y. Liu, *Adv. Mater.*, 2024, **36**, 2306772.

7 H. Y. Hou, S. Tian, H. R. Ge, J. D. Chen, Y. Q. Li and J. X. Tang, *Adv. Funct. Mater.*, 2022, **32**, 2209324.

8 W. Deng, M. Dai, C. Wang, C. You, W. Chen, S. Han, J. Han, F. Wang, M. Ye, S. Zhu, J. Cui, Q. J. Wang and Y. Zhang, *Adv. Mater.*, 2022, **34**, 2203766.

9 H. Chen, L. Su, M. Jiang and X. Fang, *Adv. Funct. Mater.*, 2017, **27**, 1704181.

10 J. Pan, Y. Wu, X. Zhang, J. Chen, J. Wang, S. Cheng, X. Wu, X. Zhang and J. Jie, *Nat. Commun.*, 2022, **13**, 6629.

11 G. Konstantatos and E. H. Sargent, *Nat. Nanotechnol.*, 2010, **5**, 391–400.

12 Y. Liu and P. Xing, *Adv. Mater.*, 2023, **35**, 2300968.

13 B. Cheng, Y. Zou and G. Song, *Opt. Laser Technol.*, 2024, **174**, 110531.

14 B. Cheng, Y. Zou and G. Song, *Opt. Commun.*, 2024, **571**, 130957.

15 X. Wang, Y. Li, L. Huang, X. Jiang, L. Jiang, H. Dong, Z. Wei, J. Li and W. Hu, *J. Am. Chem. Soc.*, 2017, **139**, 14976–14982.

16 C. Chen, L. Gao, W. Gao, C. Ge, X. Du, Z. Li, Y. Yang, G. Niu and J. Tang, *Nat. Commun.*, 2019, **10**, 1927.

17 Q. Zhao, F. Gao, H. Chen, W. Gao, M. Xia, Y. Pan, H. Shi, S. Su, X. Fang and J. Li, *Mater. Horiz.*, 2021, **8**, 3113–3123.

18 Q. Gu, J. Zha, C. Chen, X. Wang, W. Yao, J. Liu, F. Kang, J. Yang, Y. Y. Li, D. Lei, Z. Tang, Y. Han, C. Tan and Q. Zhang, *Adv. Mater.*, 2024, **36**, 2306414.

19 J. P. B. Mueller, K. Leosson and F. Capasso, *Optica*, 2016, **3**, 42.

20 L. Li, J. Wang, L. Kang, W. Liu, L. Yu, B. Zheng, M. L. Brongersma, D. H. Werner, S. Lan, Y. Shi, Y. Xu and X. Wang, *ACS Nano*, 2020, **14**, 16634–16642.

21 N. Huo and G. Konstantatos, *Adv. Mater.*, 2018, **30**, 1801164.

22 Q. Qiu and Z. Huang, *Adv. Mater.*, 2021, **33**, 2008126.

23 B. Zhang, Y. Zhang, J. Duan, W. Zhang and W. Wang, *Sensors*, 2016, **16**, 1153.

24 D. Lee, S. Y. Han, Y. Jeong, D. M. Nguyen, G. Yoon, J. Mun, J. Chae, J. H. Lee, J. G. Ok, G. Y. Jung, H. J. Park, K. Kim and J. Rho, *Sci. Rep.*, 2018, **8**, 12393.

25 S. Chen, R. Cao, X. Chen, Q. Wu, Y. Zeng, S. Gao, Z. Guo, J. Zhao, M. Zhang and H. Zhang, *Adv. Mater. Interfaces*, 2020, **7**, 1902179.

26 X. He, W. Gao, L. Xie, B. Li, Q. Zhang, S. Lei, J. M. Robinson, E. H. Hároz, S. K. Doorn, W. Wang, R. Vajtai, P. M. Ajayan, W. W. Adams, R. H. Hauge and J. Kono, *Nat. Nanotechnol.*, 2016, **11**, 633–638.

27 X. He, N. Fujimura, J. M. Lloyd, K. J. Erickson, A. A. Talin, Q. Zhang, W. Gao, Q. Jiang, Y. Kawano, R. H. Hauge, F. Léonard and J. Kono, *Nano Lett.*, 2014, **14**, 3953–3958.

28 X. Wang, N. Aroonyadet, Y. Zhang, M. Mecklenburg, X. Fang, H. Chen, E. Goo and C. Zhou, *Nano Lett.*, 2014, **14**, 3014–3022.

29 Z. Ren, P. Wang, K. Zhang, W. Ran, J. Yang, Y. Liu, Z. Lou, G. Shen and Z. Wei, *IEEE Electron Device Lett.*, 2021, **42**, 549–552.

30 Z.-M. Liao, J. Xu, J.-M. Zhang and Da.-P. Yu, *Chin. Phys. Lett.*, 2008, **25**, 2622–2624.

31 K. Zhao, J. Yang, M. Zhong, Q. Gao, Y. Wang, X. Wang, W. Shen, C. Hu, K. Wang, G. Shen, M. Li, J. Wang, W. Hu and Z. Wei, *Adv. Funct. Mater.*, 2021, **31**, 2006601.

32 X. Li, H. Liu, C. Ke, W. Tang, M. Liu, F. Huang, Y. Wu, Z. Wu and J. Kang, *Laser Photonics Rev.*, 2021, **15**, 2100322.

33 L. Li, W. Han, L. Pi, P. Niu, J. Han, C. Wang, B. Su, H. Li, J. Xiong, Y. Bando and T. Zhai, *InfoMat*, 2019, **1**, 54–73.

34 F. Xia, H. Wang and Y. Jia, *Nat. Commun.*, 2014, **5**, 4458.

35 Y. Cui, Z. Zhou, X. Wang, X. Wang, Z. Ren, L. Pan and J. Yang, *Nano Res.*, 2021, **14**, 2224–2230.

36 S. Yang, Y. Liu, M. Wu, L. Zhao, Z. Lin, H. Cheng, Y. Wang, C. Jiang, S. Wei, L. Huang, Y. Huang and X. Duan, *Nano Res.*, 2018, **11**, 554–564.

37 S. Zhao, P. Luo, S. Yang, X. Zhou, Z. Wang, C. Li, S. Wang, T. Zhai and X. Tao, *Adv. Opt. Mater.*, 2021, **9**, 2100198.

38 S. Yang, Y. Yang, M. Wu, C. Hu, W. Shen, Y. Gong, L. Huang, C. Jiang, Y. Zhang and P. M. Ajayan, *Adv. Funct. Mater.*, 2018, **28**, 1707379.

39 L. Li, W. Wang, P. Gong, X. Zhu, B. Deng, X. Shi, G. Gao, H. Li and T. Zhai, *Adv. Mater.*, 2018, **30**, 1706771.

40 D. Kim, K. Park, J. H. Lee, I. S. Kwon, I. H. Kwak and J. Park, *Small*, 2021, **17**, 2006310.

41 F. Liu, S. Zheng, X. He, A. Chaturvedi, J. He, W. L. Chow, T. R. Mion, X. Wang, J. Zhou, Q. Fu, H. J. Fan, B. K. Tay, L. Song, R. H. He, C. Kloc, P. M. Ajayan and Z. Liu, *Adv. Funct. Mater.*, 2016, **26**, 1169–1177.

42 E. Zhang, P. Wang, Z. Li, H. Wang, C. Song, C. Huang, Z. Chen, L. Yang, K. Zhang, S. Lu, W. Wang, S. Liu, H. Fang, X. Zhou, H. Yan, J. Zou, X. Wan, P. Zhou, W. Hu and F. Xiu, *ACS Nano*, 2016, **10**, 8067–8077.

43 L. Pi, C. Hu, W. Shen, L. Li, P. Luo, X. Hu, P. Chen, D. Li, Z. Li, X. Zhou and T. Zhai, *Adv. Funct. Mater.*, 2021, **31**, 2006774.

44 Y. Yang, S. Liu, W. Yang, Z. Li, Y. Wang, X. Wang, S. Zhang, Y. Zhang, M. Long, G. Zhang, D. Xue, J. Hu and L. Wan, *J. Am. Chem. Soc.*, 2018, **140**, 4150–4156.

45 L. Tong, X. Huang, P. Wang, L. Ye, M. Peng, L. An, Q. Sun, Y. Zhang, G. Yang, Z. Li, F. Zhong, F. Wang, Y. Wang, M. Motlag, W. Wu, G. J. Cheng and W. Hu, *Nat. Commun.*, 2020, **11**, 2308.

46 Y. Pan, Q. Zhao, F. Gao, M. Dai, W. Gao, T. Zheng, S. Su, J. Li and H. Chen, *ACS Appl. Mater. Interfaces*, 2022, **14**, 21383–21391.

47 L. Li, P. Gong, D. Sheng, S. Wang, W. Wang, X. Zhu, X. Shi, F. Wang, W. Han, S. Yang, K. Liu, H. Li and T. Zhai, *Adv. Mater.*, 2018, **30**, 1804541.

48 K. An, Y. Pan, X. Rong, T. Zheng, L. Li, H. Sun, J. Zeng, Y. Sang, F. Huang, D. Yue, W. J. Yoo and H. Chen, *Adv. Funct. Mater.*, 2024, 2409331.

49 T. Zheng, M. Yang, Y. Pan, Z. Zheng, Y. Sun, L. Li, N. Huo, D. Luo, W. Gao and J. Li, *ACS Appl. Mater. Interfaces*, 2023, **15**, 29363–29374.

50 J. Ahn, K. Ko, J. Kyhm, H. Ra, H. Bae, S. Hong, D. Kim, J. Jang, T. W. Kim, S. Choi, J. Kang, N. Kwon, S. Park, B. Ju, T. Poon, M. Park, S. Im and D. K. Hwang, *ACS Nano*, 2021, **15**, 17917–17925.

51 H. Wang, Y. Li, P. Gao, J. Wang, X. Meng, Y. Hu, J. Yang, Z. Huang, W. Gao, Z. Zheng, Z. Wei, J. Li and N. Huo, *Adv. Mater.*, 2024, **36**, 2309371.

52 Y. Chen, X. Wang, L. Huang, X. Wang, W. Jiang, Z. Wang, P. Wang, B. Wu, T. Lin, H. Shen, Z. Wei, W. Hu, X. Meng, J. Chu and J. Wang, *Nat. Commun.*, 2021, **12**, 4030.

53 P. K. Venuthurumilli, P. D. Ye and X. Xu, *ACS Nano*, 2018, **12**, 4861–4867.

54 T. Chiou, S. Kleinlogel, T. Cronin, R. Caldwell, B. Loeffler, A. Siddiqi, A. Goldizen and J. Marshall, *Curr. Biol.*, 2008, **18**, 429–434.

55 A. Maiti and A. J. Pal, *Angew. Chem., Int. Ed.*, 2022, **61**, e202214161.

56 M. D. Ward, W. Shi, N. Gasparini, J. Nelson, J. Wade and M. J. Fuchter, *J. Mater. Chem. C*, 2022, **10**, 10452–10463.

57 M. Dai, C. Wang, B. Qiang, F. Wang, M. Ye, S. Han, Y. Luo and Q. J. Wang, *Nat. Commun.*, 2022, **13**, 4560.

58 X. Yang, X. Gao, Y. Zheng, H. Kuang, C. Chen, M. Liu, P. Duan and Z. Tang, *CCS Chem.*, 2023, **5**, 2760–2789.

59 K. Yao and Y. Liu, *Nanoscale*, 2018, **10**, 8779–8786.

60 J. Ahn, E. Lee, J. Tan, W. Yang, B. Kim and J. Moon, *Mater. Horiz.*, 2017, **4**, 851–856.

61 B. Ranjbar and P. Gill, *Chem. Biol. Drug Des.*, 2009, **74**, 101–120.

62 D. M. Rogers, S. B. Jasim, N. T. Dyer, F. Auvray, M. Réfrégiers and J. D. Hirst, *Chem*, 2019, **5**, 2751–2774.

63 X. Jiang, Y. Ji, F. Fan, S. Jiang, Z. Tan, H. Zhao, J. Cheng and S. Chang, *Photonics Res.*, 2023, **11**, 1880.

64 R. Kuroda and T. Honma, *Chirality*, 2000, **12**, 269–277.

65 F. Furlan, J. M. Moreno-Naranjo, N. Gasparini, S. Feldmann, J. Wade and M. J. Fuchter, *Nat. Photonics*, 2024, **18**, 658–668.

66 Á. Jiménez-Galán, R. E. F. Silva, O. Smirnova and M. Ivanov, *Nat. Photonics*, 2020, **14**, 728–732.

67 W. Li, Z. J. Coppens, L. V. Besteiro, W. Wang, A. O. Govorov and J. Valentine, *Nat. Commun.*, 2015, **6**, 8379.

68 G. Long, R. Sabatini, M. I. Saidaminov, G. Lakhwani, A. Rasmita, X. Liu, E. H. Sargent and W. Gao, *Nat. Rev. Mater.*, 2020, **5**, 423–439.

69 X. Shang, L. Wan, L. Wang, F. Gao and H. Li, *J. Mater. Chem. C*, 2022, **1**, 24–241.

70 J. Cai, W. Zhang, L. Xu, C. Hao, W. Ma, M. Sun, X. Wu, X. Qin, F. M. Colombari, A. F. de Moura, J. Xu, M. C. Silva, E. B. Carneiro-Neto, W. R. Gomes, R. A. L. Vallée, E. C. Pereira, X. Liu, C. Xu, R. Klajn, N. A. Kotov and H. Kuang, *Nat. Nanotechnol.*, 2022, **17**, 408–416.

71 Y. Yang, R. C. Da Costa, M. J. Fuchter and A. J. Campbell, *Nat. Photonics*, 2013, **7**, 634–638.

72 Y. Liu, Z. Li, M. Wang, J. Chan, G. Liu, Z. Wang and W. Jiang, *J. Am. Chem. Soc.*, 2024, **146**, 5295–5304.

73 A. Ishii and T. Miyasaka, *Sci. Adv.*, 2020, **6**, eabd3274.

74 C. Chen, L. Gao, W. Gao, C. Ge, X. Du, Z. Li, Y. Yang, G. Niu and J. Tang, *Nat. Commun.*, 2019, **10**, 1927.

75 C. Niu, S. Huang, N. Ghosh, P. Tan, M. Wang, W. Wu, X. Xu and P. D. Ye, *Nano Lett.*, 2023, **23**, 3599–3606.

76 S. Wang, D. Li, M. Zha, X. Yan, Z. Liu and J. Tian, *ACS Nano*, 2023, **17**, 16230–16238.

77 X. Su, T. Huang, J. Wang, Y. Liu, Y. Zheng, Y. Shi and X. Wang, *Acta Phys. Sin.*, 2021, **70**, 138501.

78 X. Sun, S. Velez, A. Atxabal, A. Bedoya-Pinto, S. Parui, X. Zhu, R. Llopis, F. Casanova and L. E. Hueso, *Science*, 2017, **357**, 677–680.

79 K. Bairagi, D. G. Romero, F. Calavalle, S. Catalano, E. Zuccatti, R. Llopis, F. Casanova and L. E. Hueso, *Adv. Mater.*, 2020, **32**, 1906908.

80 C. C. Fan, X. B. Han, B. D. Liang, C. Shi, L. P. Miao, C. Y. Chai, C. D. Liu, Q. Ye and W. Zhang, *Adv. Mater.*, 2022, **34**, 2204119.

81 C. Cheon, Z. Sun, J. Cao, J. F. G. Marin, M. Tripathi, K. Watanabe, T. Taniguchi, M. Luisier and A. Kis, *npj 2D Mater. Appl.*, 2023, **7**, 74.

82 J. Wang, H. Lu, X. Pan, J. Xu, H. Liu, X. Liu, D. R. Khanal, M. F. Toney, M. C. Beard and Z. V. Vardeny, *ACS Nano*, 2021, **15**, 588–595.

83 S. Duan, F. Qin, P. Chen, X. Yang, C. Qiu, J. Huang, G. Liu, Z. Li, X. Bi, F. Meng, X. Xi, J. Yao, T. Ideue, B. Lian, Y. Iwasa and H. Yuan, *Nat. Nanotechnol.*, 2023, **18**, 867–874.

84 J. Ma, Q. Gu, Y. Liu, J. Lai, P. Yu, X. Zhuo, Z. Liu, J. Chen, J. Feng and D. Sun, *Nat. Mater.*, 2019, **18**, 476–481.

85 Z. Ni, K. Wang, Y. Zhang, O. Pozo, B. Xu, X. Han, K. Manna, J. Paglione, C. Felser, A. G. Grushin, F. de Juan, E. J. Mele and L. Wu, *Nat. Commun.*, 2021, **12**, 154.

86 M. Eginligil, B. Cao, Z. Wang, X. Shen, C. Cong, J. Shang, C. Soci and T. Yu, *Nat. Commun.*, 2015, **6**, 7636.

87 K. Ando, M. Morikawa, T. Trypiniotis, Y. Fujikawa, C. H. W. Barnes and E. Saitoh, *Appl. Phys. Lett.*, 2010, **96**, 82502.

88 M. Qi and Z. Hongwu, *Physics*, 2013, **42**, 54.

89 K. Ando and E. Saitoh, *Nat. Commun.*, 2012, **3**, 629.

90 S. K. Khamari, S. Porwal, S. M. Oak and T. K. Sharma, *Appl. Phys. Lett.*, 2015, **107**, 072108.

91 K. Wang, B. Zhang, C. Yan, L. Du and S. Wang, *Nat. Commun.*, 2024, **15**, 9036.

92 S. H. Liang, Y. Lu and X. F. Han, *Acta Phys. Sin.*, 2020, **69**, 208501.

93 R. S. Joshya, H. Carrère, V. G. Ibarra-Sierra, J. C. Sandoval-Santana, V. K. Kalevich, E. L. Ivchenko, X. Marie, T. Amand, A. Kunold and A. Balocchi, *Adv. Funct. Mater.*, 2021, **31**, 2102003.

94 D. Lagarde, L. Lombez, X. Marie, A. Balocchi, T. Amand, V. K. Kalevich, A. Shiryaev, E. Ivchenko and A. Egorov, *Phys. Status Solidi A*, 2007, **204**, 208–220.

95 L. Lombez, P. F. Braun, H. Carrère, B. Urbaszek, P. Renucci, T. Amand, X. Marie, J. C. Harmand and V. K. Kalevich, *Appl. Phys. Lett.*, 2005, **87**, 252115.

96 V. G. Ibarra-Sierra, J. C. Sandoval-Santana, R. S. Joshya, H. Carrère, L. A. Bakaleinikov, V. K. Kalevich, E. L. Ivchenko, X. Marie, T. Amand, A. Balocchi and A. Kunold, *Phys. Rev. Appl.*, 2021, **15**, 64040.

97 M. Jung, S. Dutta-Gupta, N. Dabidian, I. Brener, M. Shcherbakov and G. Shvets, *ACS Photonics*, 2018, **5**, 4283–4288.

98 J. Bai, C. Wang, X. Chen, A. Basiri, C. Wang and Y. Yao, *Photonics Res.*, 2019, **7**, 1051.

99 E. Arbabi, S. M. Kamali, A. Arbabi and A. Faraon, *ACS Photonics*, 2018, **5**, 3132–3140.

100 A. Basiri, X. Chen, J. Bai, P. Amrollahi, J. Carpenter, Z. Holman, C. Wang and Y. Yao, *Light: Sci. Appl.*, 2019, **8**, 78.

101 X. Tu, S. Mceldowney, Y. Zou, M. Smith, C. Guido, N. Brock, S. Miller, L. Jiang and S. Pau, *Appl. Opt.*, 2020, **59**, G33–G40.

102 J. Zuo, J. Bai, S. Choi, A. Basiri, X. Chen, C. Wang and Y. Yao, *Light: Sci. Appl.*, 2023, **12**, 218.

103 N. A. Rubin, G. D. Aversa, P. Chevalier, Z. Shi, W. T. Chen and F. Capasso, *Science*, 2019, **365**.

104 C. Zhang, J. Hu, Y. Dong, A. Zeng, H. Huang and C. Wang, *Photonics Res.*, 2021, **9**, 583.

105 B. Cheng, Y. Zou and G. Song, *Photonics*, 2024, **11**, 571.

106 Y. Zhao, Y. Qiu, J. Feng, J. Zhao, G. Chen, H. Gao, Y. Zhao, L. Jiang and Y. Wu, *J. Am. Chem. Soc.*, 2021, **143**, 8437–8445.

107 J. Ma, C. Fang, L. Liang, H. Wang and D. Li, *Small*, 2021, **17**, 2103855.

108 M. Che, B. Wang, X. Zhao, Y. Li, C. Chang, M. Liu, Y. Du, L. Qi, N. Zhang, Y. Zou and S. Li, *ACS Nano*, 2024, **18**, 30884–30895.

109 C. Wang, G. Li, Z. Dai, W. Tian and L. Li, *Adv. Funct. Mater.*, 2024, **34**, 2316265.

110 Y. Zhao, Z. Zhou, X. Liu, A. Ren, S. Ji, Y. Guan, Z. Liu, H. Liu, P. Li, F. Hu and Y. S. Zhao, *Adv. Opt. Mater.*, 2023, **11**, 2301239.

111 C. Ma, S. Yuan, P. Cheung, K. Watanabe, T. Taniguchi, F. Zhang and F. Xia, *Nature*, 2022, **604**, 266–272.

112 Q. Fan, W. Xu, X. Hu, W. Zhu, T. Yue, F. Yan, P. Lin, L. Chen, J. Song, H. J. Lezec, A. Agrawal, Y. Lu and T. Xu, *Nat. Commun.*, 2023, **14**, 7180.

113 J. S. Tyo, D. L. Goldstein, D. B. Chenault and J. A. Shaw, *Appl. Opt.*, 2006, **45**, 5453–5469.

114 R. Patel, A. Khan, R. Quinlan and A. N. Yaroslavsky, *Cancer Res.*, 2014, **74**, 4685–4693.

115 K. P. Gurton, A. J. Yuffa and G. W. Videen, *Opt. Lett.*, 2014, **39**, 3857–3859.

116 J. Zhong, J. Yu, L. Cao, C. Zeng, J. Ding, C. Cong, Z. Liu and Y. Liu, *Nano Res.*, 2020, **13**, 1780–1786.

117 J. Zhang, J. Zhao, Y. Zhou, Y. Wang, K. S. Blankenagel, X. Wang, M. Tabassum and L. Su, *Adv. Opt. Mater.*, 2021, **9**, 2100524.

118 Y. Hao, T. Hang, C. Chen, C. Zhang, Y. Chen, C. Yu, S. Wu, J. Yang, Z. Yang, X. Li and G. Cao, *Adv. Funct. Mater.*, 2024, 2416475.

119 S. Wu, J. Deng, X. Wang, J. Zhou, H. Jiao, Q. Zhao, T. Lin, H. Shen, X. Meng, Y. Chen, J. Chu and J. Wang, *Nat. Commun.*, 2024, **15**, 8743.

120 N. C. Wilson, E. Shin, R. E. Bangle, S. B. Nikodemski, J. H. Vella and M. H. Mikkelsen, *Nano Lett.*, 2023, **23**, 8547–8552.

121 Z. Zhang, S. Wang, C. Liu, R. Xie, W. Hu and P. Zhou, *Nat. Nanotechnol.*, 2022, **17**, 27–32.

122 F. Wang, S. Zhu, W. Chen, J. Han, R. Duan, C. Wang, M. Dai, F. Sun, Y. Jin and Q. J. Wang, *Nat. Nanotechnol.*, 2024, **19**, 455–462.

123 Y. Yu, T. Xiong, Z. Zhou, D. Liu, Y. Liu, J. Yang and Z. Wei, *Nano Lett.*, 2024, **24**, 6788–6796.

124 X. Wang, Z. Dou, C. Zhang, F. Deng, X. Lu, S. Wang, L. Zhou and T. Ding, *Nanophotonics*, 2022, **11**, 1003–1009.